IEEE Access
Multidisciplinary | Rapid Review | Open Access Journal

Received September 10, 2020, accepted September 21, 2020, date of publication September 28, 2020,
date of current version October 7, 2020.

Digital Object Identifier 10.1109/ACCESS.2020.3027066

Multi-Degree of Freedom Isolation System With High Frequency Roll-Off for Drone Camera Stabilization

MOHIT VERMA[1], VICENTE LAFARGA[2], THOMAS DEHAEZE[3], AND CHRISTOPHE COLLETTE[2,3]
[1]CSIR-Structural Engineering Research Centre, Chennai 600113, India
[2]Precision Mechatronics Laboratory, BEAMS Department, Université Libre de Bruxelles, 1050 Brussels, Belgium
[3]Department of Aerospace and Mechanical Engineering, University of Liège, 4000 Liège, Belgium

Corresponding author: Mohit Verma (mohitverma@serc.res.in)

This work was supported by the Wallonie Region (WALInnov Project Trusteye) under Grant 1710040.

ABSTRACT The technological developments in the field of image based sensing have led to a vast growth in the use of drones in various domains. The drone is usually equipped with an image sensor (camera) which collect images over the target area. These images are then post-processed to extract the important information. Efficiency and accuracy of the image based sensing are largely dependent on the captured image quality. Therefore, it is important to prevent the transmission of the drone vibrations to the camera. Most of the current camera mounting systems use passive rubber mounts for isolation. However, these mounts are effective only in vertical direction and essentially adds damping to the system which degrades the performance of the isolation at high frequency. In this paper, a multi-degree of freedom isolation system, based on a Stewart platform configuration, is proposed for drone camera stabilization. The important features of the proposed isolation system are — (i) high frequency roll-off, (ii) no use of flexible joints, (iii) uses non-contact voice coil actuator thus avoiding spurious resonances of the legs, (iv) adjustable stiffness, (v) 3D printed lightweight parts and (vi) centralized control using a single sensor (inertial measurement unit). A prototype of the proposed system has been manufactured and validated experimentally. The proposed isolation system is found to reduce the response of the isolation system near resonance without compromising performance at high frequency. The application of the isolation system can be easily extended to other fields which require high quality image acquisition.

INDEX TERMS Vibration isolation, Stewart platform, hexapod, active control, image stabilization.

I. INTRODUCTION

The recent years have seen a vast growth in the use of image based sensing technologies using drones. Drone based sensing systems offer simple and low-cost solutions which find applications in health monitoring [1], precision agriculture [2], military surveillance [3] and remote sensing [4]. The drone is equipped with an image sensor (camera) which collects high resolution images during its flight over a localized region. The images captured by the drone are then post-processed to extract some useful information. The effectiveness of image based sensing is determined by the captured image quality. The vibrations on the camera can cause blurring of the captured images. Therefore, there is a need to prevent the transmission of drone vibrations to the camera. This can be achieved through stabilization system for camera, which can developed using either passive or active elements.

Passive systems are purely mechanical. Earlier studies claimed that a simple linear spring-mass dashpot system can be used as passive isolation for camera [5]. Kienholz *et al.* [6] proposed damping system for optical payloads. The damper dissipated the energy through eddy current. All metal design, insensitivity to temperature, linear behaviour, no fluids and its robustness makes it a good choice for space applications. A camera mount based on dry-friction isolator was developed by Gjika and Dufour [7]. A passive vibration abatement system was proposed by Fernandez *et al.* [8] which utilized sprung-mass isolation technique. The system was claimed to work for high-frequency vibrations (greater than 2 Hz) in the horizontal plane. Qian *et al.* [9] proposed an irrotational displacement isolator to prevent rocking of the payload. The device used double parallelogram linkage mechanism

The associate editor coordinating the review of this manuscript and approving it for publication was Giambattista Gruosso.

to restrain the rotation and allow only axial motion of the payload with respect to the aircraft. A new kind of passive system based on bio mimetic, inspired by avian, was proposed by [10]. This type of isolation system is best suited for drones using a flapping mechanism.

A hybrid isolation system, incorporating a vibration absorber, was proposed by Webster and Semke [11]. The damping of the system was enhanced by using viscoelastic materials. Meas *et al.* [12] presented ian solation system using wire rope for the pan-tilt-zoom camera system. A three axis accelerometer was connected to the body of the aircraft to measure these disturbances. The disturbances were recorded under different operating conditions of the aircraft like flying, rolling, take off and landing. The wire-rope isolators were found to be effective in the vertical direction. The vibration reduction in the other two directions were not significant.

Active image stabilization systems use sensors to measure the motion and then an actuating system to compensate for it. Active system are found to be effective for a broader range of frequencies as they are adaptive in nature [13]–[15]. They are able to compensate for a wider range of disturbances. This section presents some of the active stabilization systems that have been developed for mechanical camera stabilization. Marichal *et al.* [16] designed a low-cost platform, for mounting a camera on an unmanned aerial vehicle (UAV). The controller used was based on artificial neuro-fuzzy inference system (ANFIS). The semi-active strategy was proposed using a spring-mass-damper system with time varying damping. The motion of the platform was controlled only on two-axis. Stuckel *et al.* [17], Stuckel and Semke [18] developed a mount using just the piezoelectric actuators. This system was developed for high-frequency oscillations having small amplitude.

Sumathy *et al.* [19] used a piezoelectric mount to actively cancel the vibration generated from the quadcopter. The performance of the three different types of algorithms were compared — Least Mean Square (LMS), Filtered-X-Least Mean Square (FxLMS) and Normalized Least Mean Square (NLMS). The NLMS algorithm performed best among the studied algorithms. Oh *et al.* [20], [21] and Park and Choi [22] developed camera mounts using piezostack actuators. The vibration levels were found to be reduced up to 78% near the critical frequencies. Lee *et al.* [23] proposed active vibration isolation using piezoelectric unimorph with mechanically pre-stressed substrate (PUMPS). The active isolation system was developed for removing the jitter and improving the quality of image acquisition by optical payloads. Two different control schemes were used — positive position feedback (PPF) and negative velocity feedback (NVF).

Baer and Semke [24] developed a frictionless camera mount using composite plates and magnets. The isolation was able to counteract against the small attitude deflections. Gasteratos [25] presented a new scheme for a pan/tilt camera for using fuzzy-grey controller. Gyros were used for controlling the pan and tilt of the camera. The performance of the proposed controller was compared with that of the PID. Fuzzy-grey controller was found to perform better and was able to provide better image stabilization.

This article focuses on the development of a multi-degree of freedom vibration isolation system for stabilizing cameras installed on drones. The proposed isolation system is based on a Stewart platform configuration. Premount *et al.* [26] proposed a Stewart platform configuration using voice coil actuators and flexible joints. The unique feature of the design was that the mass of the magnets was moved from the leg to the bottom platform. Also, the membrane inside the voice coil served as a flexible joint. Zheng *et al.* [27] proposed a passive Stewart platform configuration using negative stiffness magnetic springs. The platform was designed to have high static and low dynamic stiffness. Wu *et al.* [28] proposed another passive Stewart platform using X-shape structures as legs. He *et al.* [29] proposed a 18-legged inertially stabilized Stewart platform for protecting navigation systems from external shocks. Wang *et al.* [30] developed a Stewart platform using piezoelectric actuators for micro-vibration isolation. Yang *et al.* [31] proposed an isolation system for space precision system. They also developed the control strategy to compensate for the parasitic stiffness induced due to flexible joints.

The conventional configurations of Stewart platforms suffer from two major drawbacks. The first is the spurious resonances in the legs of the platform. The mass and stiffness of the legs are significant and can result in spurious resonances which degrades the performance of the isolation. The second major drawback is the flexible joints which amount to parasitic stiffness. The friction and the backlash in the joints are another matter of concern while designing the controls for the platform. In this article, we propose some design modifications to overcome the drawbacks of the conventional Stewart platform configuration. More specifically, the platform is designed for drone camera stabilization. The nature of the drone vibrations is high frequency and low-amplitude. Therefore, it is desired to have an isolation system with high frequency roll-off. The proposed configurations uses non-contact voice coil actuators. Also, there are no flexible joints in the proposed system. A very simple control architecture is used for active isolation using centralized control. The parts of the platform are manufactured using 3D printing technology. The top and the bottom platform are interconnected using three springs. Unlike most of the Stewart platforms, the stiffness of the proposed system can be adjusted to account for different payloads.

The organization of the manuscript is as follows. Section II describes the design features of the proposed isolation system. A dynamic model of the proposed isolation system is presented in Section III. The design of the prototype isolation system is described in Section IV. The control design strategy for active isolation is presented in Section V. The details of the experiments conducted on a prototype to assess the performance of the isolator are presented in Section VI. This is followed by concluding remarks in Section VII.

II. DESIGN DESCRIPTION

In the present study, an active isolation system based on the cubic configuration of a Stewart platform is proposed. The configuration of the isolation system has been modified for specifically for drone camera stabilization. This section describes the changes made to the conventional Stewart platform configuration and also highlights the motivation behind these changes.

(i) **Non-contact actuators**: In most of the Stewart platform configurations, the payload and bottom platform are connected with the help of struts which results in spurious resonances at high frequencies. Since the nature of the drone vibration is low amplitude and high frequency [32], spurious resonance can severely degrade the performance of the isolation system. To overcome the problem of spurious resonances in the legs, it is proposed to use non-contact voice coil actuators in the legs of the isolation such that there is no stiffness in the legs. The top and bottom platform are supported on three springs. Figure 1 shows the configuration of the proposed isolation system.

(ii) **No flexible joints**: The conventional rotational joints suffers from the problem of friction and backlash. On the other hand, flexible joints add parasitic stiffness which degrades the isolation performance. The modified design eliminates the need for rotational or flexible joints. Instead, the radial clearance between the coil and the permanent magnet is increased to allow for the rotation of the top platform (see Figure 2).

(iii) **Lightweight**: The weight of the drone unit needs to comply with the air traffic regulations. Adding too much weight might interfere with the navigation controls. It may also lead to increased power consumption by the drone. For light weight design requirement, the actuator housing assembly is 3D printed using poly lactic acid (PLA) material, which offers high resilience and durability.

(iv) **Compactness**: The isolation system needs to have a compact footprint so that it can be combined with existing drone-camera systems. There is also a constraint on the height of the isolation. This again is achieved by using non-contact actuators without any flexible joints.

(v) **Control architecture**: The compact nature of the isolation system does not leave much room for the placement of the large number of sensors. Usually force sensors or accelerometers are collocated with the actuators in the legs of the isolation. It is proposed to use only one sensor — inertial measurement unit (IMU).

(vi) **Modular**: The designed isolation system should be modular. It should be compatible with different drone-camera systems. This is facilitated by the design of special fasteners which can be used to adjust the spring stiffness between the top and bottom platform. The isolation system works like a module and can be adapted for different payloads (camera systems).

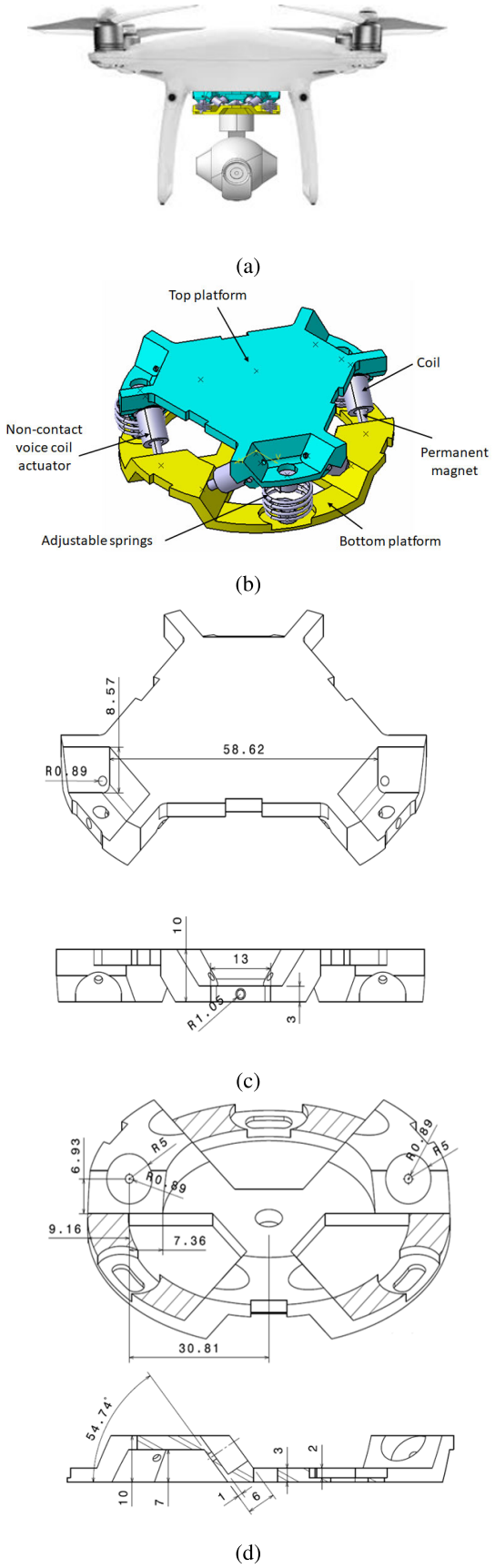

FIGURE 1. Proposed isolation system– (a) integrated system, (b) configuration, (c) top platform and (d) bottom platform.

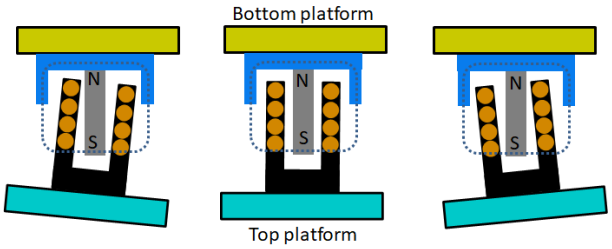

FIGURE 2. Radial clearance between the coil and the magnet allows the rotation of the top platform.

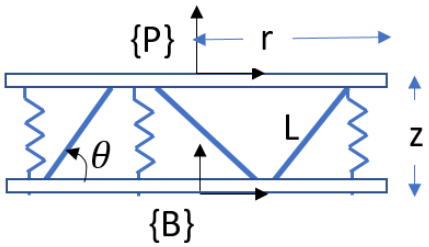

FIGURE 3. Geometry of the isolation system.

III. DYNAMIC MODEL OF THE ISOLATION SYSTEM

A Stewart platform has authority over six degrees of freedom. The present configuration of the isolation system consists of six non-contact voice coil actuators. The top and bottom platforms are connected by three springs. This section presents the formulation of a dynamic model for the proposed isolator.

A. GEOMETRIC CONFIGURATION

The actuators are arranged in a cubic configuration. The cubic configuration of a Stewart platform has equal control authority in all the degrees of freedom [33]. The velocities of the isolation legs are related to the velocities of the payload plate by a Jacobian matrix (refer equations (13) and (23)). Since the application is intended to suppress low amplitude motion, the Jacobian remains constant. This makes it possible to use the nominal configuration to evaluate the Jacobian matrix.

For the cubic configuration (see Fig. 3), the inclination angle of the leg with the vertical plane is constant and is equal to

$$\theta = \tan^{-1}\left(\frac{1}{\sqrt{2}}\right) \tag{1}$$

The height, z, and radius, r of the platform are related by the following equation

$$\frac{r}{L} = \cos\theta = \sqrt{\frac{2}{3}}; \frac{z}{L} = \sin\theta = \sqrt{\frac{1}{3}} \tag{2}$$

B. FRAMES OF REFERENCE

Three different frames of reference are selected for the dynamic modelling of the proposed isolation system

(i) Global frame of reference, $\{B\}$ — which coincides with the centre of mass of the bottom platform.
(ii) Payload frame of reference, $\{P\}$ — which is the fixed to the centre of mass of the top plate.
(iii) Local frame of reference — which is attached to the corresponding spring and the the actuator leg.

C. POSITION OF THE SENSOR AND ACTUATORS

The location of the sensor and the actuators is shown in Figure 4. The actuator legs are shown in the encircled numbers. IMU is placed at the origin of the payload frame of reference. The coordinates of the position of different points in the global frame of reference are summarized in Table 1.

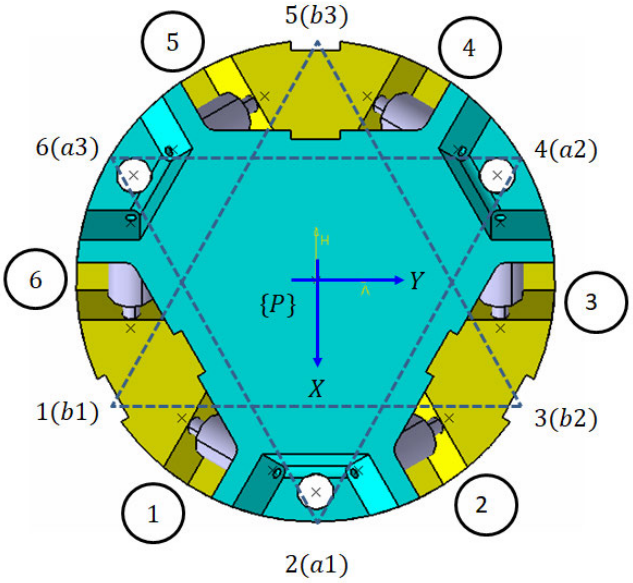

FIGURE 4. Location of the sensor and actuators.

TABLE 1. Location of sensor and actuator in global frame of reference.

S. No.	Point	X	Y	Z
1	b1	$r/2$	$-r\sqrt{3}/2$	0
2	a1	r	0	z
3	b2	$r/2$	$r\sqrt{3}/2$	0
4	a2	$-r/2$	$r\sqrt{3}/2$	z
5	b3	$-r$	0	0
6	a3	$-r/2$	$-r\sqrt{3}/2$	z
7	B	0	0	0
8	P	0	0	z

D. MODELLING OF THE SPRINGS

For modelling of the springs, it is assumed that the bottom platform is fixed and the payload platform is subjected to the forces and moments acting at its centre of mass (see Figure 5). Let the motion of the payload plate in the $\{B\}$ frame of reference be given by

$$X = \begin{bmatrix} x & y & z & \theta_x & \theta_y & \theta_z \end{bmatrix}^T$$

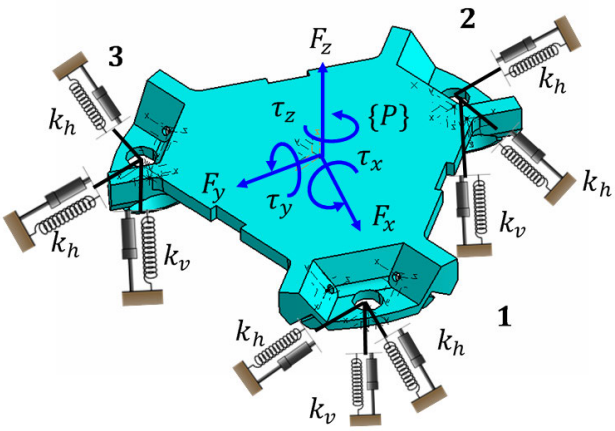

FIGURE 5. Modelling of the springs in isolation system.

The displacement of the i^{th} spring in $\{B\}$ frame of reference is given by

$$\chi_i = \begin{bmatrix} x_i & y_i & z_i \end{bmatrix}^T$$

The stiffness of the springs in the horizontal direction can be written as k_h and in vertical direction as k_v. That is, the spring stiffness in X- and Y-directions is k_h and in the Z-direction is k_v with respect to $\{B\}$ frame of reference. The forces acting on the centre of mass of the payload plate in $\{B\}$ frame of reference can be written as

$$F_{ext} = \begin{bmatrix} F & \tau \end{bmatrix} = \begin{bmatrix} F_x & F_y & F_z & \tau_x & \tau_y & \tau_z \end{bmatrix}$$

where F_x, F_y, F_z are the forces and τ_x, τ_y, τ_z are the moments. The translation motion of the payload is related to the motion of the points where springs are attached by the following relations

$$x = \frac{x_1 + x_2 + x_3}{3}; y = \frac{y_1 + y_2 + y_3}{3}; z = \frac{z_1 + z_2 + z_3}{3} \quad (3)$$

where (x_i, y_i, z_i) are the translations of point i $(i = 1, 2, 3)$ in Figure 5. If the springs are identical, the motion of the point where the springs are attached is equal to the motion of the payload in the respective direction. Hence, the effective stiffness due to springs in the X-, Y- and Z-directions is equal to $3k_h$, $3k_h$ and $3k_v$, respectively.

For rotation about X-axis, the spring 1 is fixed while the springs 2 and 3 moves in the opposite directions. Since the spring stiffness is same, the magnitude of the displacement of springs 2 and 3 is also the same (i.e., $z_2 = z_3$). From Figure 6, it can be deduced that

$$\theta_x = \frac{2z_2}{r\sqrt{3}} = \frac{2z_3}{r\sqrt{3}} \quad (4)$$

Using moment equilibrium along X-axis, we get

$$\tau_x = k_{\theta_x}\theta_x = k_v z_2 \frac{r\sqrt{3}}{2} + k_v z_3 \frac{r\sqrt{3}}{2} \quad (5)$$

Therefore, the effective stiffness along the θ_x-direction is given by

$$k_{\theta_x} = \frac{3k_v r^2}{2} \quad (6)$$

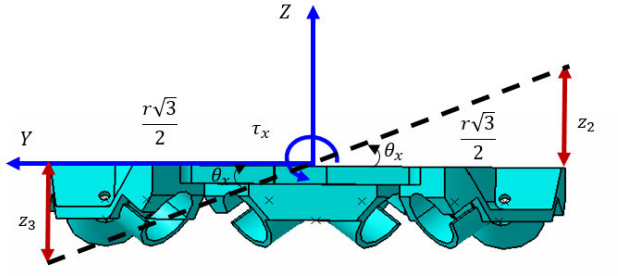

FIGURE 6. Isolation stiffness calculation in θ_x-direction.

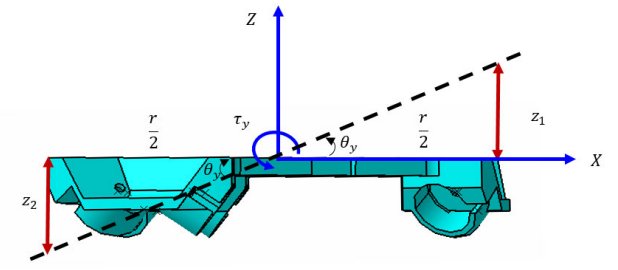

FIGURE 7. Isolation stiffness calculation in θ_y-direction.

Similarly, for the rotation about the Y-axis, spring 1 moves in the upward direction while springs 2 and 3 moves downwards (see Figure 7). The angle of rotation and the displacements of the spring are related by the following equation

$$\theta_y = \frac{z_1}{r} = \frac{2z_2}{r} = \frac{2z_3}{r} \quad (7)$$

Using moment equilibrium along the Y-direction, we get

$$\tau_y = k_{\theta_y}\theta_y = k_v z_1 r + k_v z_2 \frac{r}{2} + k_v z_3 \frac{r}{2} \quad (8)$$

The effective stiffness along the θ_y-direction is equal to

$$k_{\theta_y} = \frac{3k_v r^2}{2} \quad (9)$$

The rotation about the Z-axis results in the displacement of the springs in the X-Y plane. From Figure 8, we can write

$$\theta_z = \frac{y_1}{r} = \frac{x_2}{r} = \frac{x_3}{r} \quad (10)$$

The moment equilibrium in the Z-direction results in

$$\tau_z = k_{\theta_z}\theta_z = k_h y_1 r + k_h x_2 r + k_h x_3 r \quad (11)$$

The effective stiffness along the θ_z-direction is equal to

$$k_{\theta_z} = 3k_h r^2 \quad (12)$$

E. KINEMATIC MODELLING OF THE LEGS

The procedure described in [33] is followed for the kinematic modelling of the legs. Let R be the rotation matrix relating the frame of reference $\{P\}$ to $\{B\}$. The frame $\{B\}$ is assumed to be fixed. The definition of the various vectors shown in Figure 9 is given below

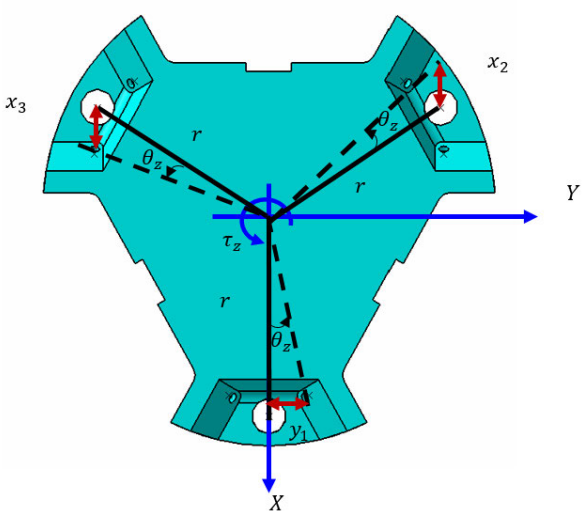

FIGURE 8. Isolation stiffness calculation in θ_z-direction.

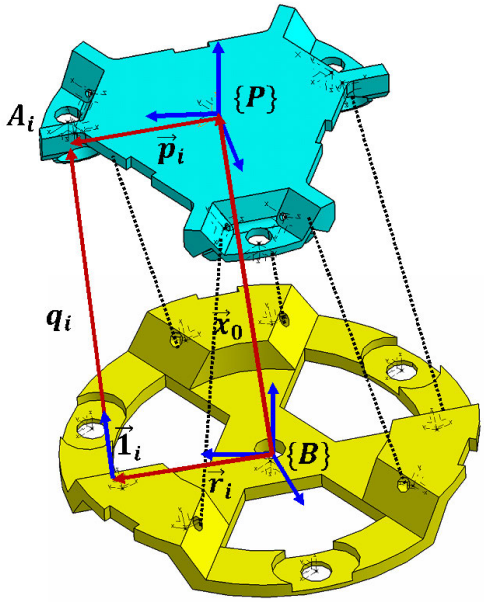

FIGURE 9. Vector representation of the isolation system for calculation of the Jacobian matrix.

- $\vec{x}_o$ Vector connecting origin of $\{B\}$ to $\{P\}$
- $\vec{p}_i$ Vector connecting origin of $\{P\}$ to the actuator in leg i on the payload plate
- $\vec{r}_i$ Vector connecting origin of $\{B\}$ to the actuator in leg i on the bottom plate
- $\vec{q}_i$ Vector connecting the attachment point of leg i in the payload and bottom plates
- $\vec{1}_i$ Unit vector along the direction of leg i

Let J be the Jacobian matrix which relates the leg's velocities to the velocity of the centre of mass of the payload plate. That is

$$\dot{q} = J\dot{X} \tag{13}$$

The absolute velocity of the point A_i on the payload plate is given by

$$\vec{v}_i = \vec{v} + \vec{\omega} \times \vec{p}_i \tag{14}$$

where $\vec{v}$ and $\vec{\omega}$ are the absolute velocity and the angular velocity of the centre of mass of the payload plate. The projection of the velocity vector along the direction of leg is given by

$$\vec{q}_i = \vec{1}_i.(\vec{v} + \vec{\omega} \times \vec{p}_i) = \vec{1}_i \cdot \vec{v} - \vec{1}_i.\vec{p}_i \times \vec{\omega} \tag{15}$$

The above equation can be expressed in the matrix form

$$\vec{q}_i = 1_i^T.v - 1_i^T.\tilde{p}_i.\omega \tag{16}$$

where $\tilde{p}$ is a skew symmetric matrix calculated from $\vec{p}$ to express the cross product and is equal to

$$\tilde{p} = \begin{bmatrix} 0 & -p_3 & p_2 \\ p_3 & 0 & -p_1 \\ -p_2 & p_1 & 0 \end{bmatrix}$$

Combining the velocities of all the legs,

$$\dot{q} = \begin{pmatrix} \cdots & \cdots \\ 1_i^T & -1_i^T\tilde{p}_i \\ \cdots & \cdots \end{pmatrix} \begin{pmatrix} v \\ \omega \end{pmatrix} \tag{17}$$

From Figure 9, it can be seen that

$$\vec{q}_i = (\vec{x}_o - \vec{r}_i) + \vec{p}_i \tag{18}$$

Projecting vectors $\vec{x}_o, \vec{r}_i$ in the frame $\{P\}$ we get

$$\vec{q}_i = R^T(\vec{x}_o - \vec{r}_i) + \vec{p}_i \tag{19}$$

The unit vector along the leg of the actuator can be written as

$$\vec{1}_i = \frac{\vec{q}_i}{|q_i|} = \frac{1}{L}\left(R^T(\vec{x}_o - \vec{r}_i) + \vec{p}_i\right) \tag{20}$$

And also,

$$1_i^T.\tilde{p}_i = \frac{1}{L}R^T(x_o - r_i)\tilde{p}_i \tag{21}$$

For small rotations of the payload plate, the rotation matrix can be approximates as an identity matrix. The Jacobian matrix for small rotations can be approximated as

$$J = \begin{pmatrix} \cdots & \cdots \\ \frac{1}{L}\left((x_o - r_i)^T\mathbf{I} + p_i^T\right) & -\frac{1}{L}(x_o - r_i)^T\mathbf{I}\tilde{p}_i \\ \cdots & \cdots \end{pmatrix} \tag{22}$$

where $\mathbf{I}$ is identity matrix of appropriate size.

The Jacobian matrix obtained by substituting the vectors of the actuator legs and joint positions is

$$J = \begin{bmatrix} 1/\sqrt{6} & 1/\sqrt{2} & 1/\sqrt{6} & 0 & -L\sqrt{2}/3 & L/\sqrt{3} \\ 1/\sqrt{6} & -1/\sqrt{2} & 1/\sqrt{6} & 0 & -L\sqrt{2}/3 & -L/\sqrt{3} \\ -2/\sqrt{6} & 0 & 1/\sqrt{6} & L/\sqrt{6} & L/\sqrt{6} & L/\sqrt{3} \\ 1/\sqrt{6} & 1/\sqrt{2} & 1/\sqrt{6} & L/\sqrt{6} & L/\sqrt{6} & -L/\sqrt{3} \\ 1/\sqrt{6} & -1/\sqrt{2} & 1/\sqrt{6} & -L/\sqrt{6} & L/\sqrt{6} & L/\sqrt{3} \\ -2/\sqrt{6} & 0 & 1/\sqrt{6} & -L/\sqrt{6} & L/\sqrt{6} & -L/\sqrt{3} \end{bmatrix} \tag{23}$$

TABLE 2. List of various components of the isolation system.

Component	Description
Actuator	Linear non-contact voice coil actuator, Model: Moticont LVCM-010-013-01, Stroke: 6.4 mm (Tolerance:±0.01 mm)
Sensor	5 DOF Inertial Measurement Unit, 2 x gyro sensor and a 3-axis accelerometer, Accelerometer sensitivity: 300mV/g (Tolerance:±1%), Gyro raw sensitivity: 0.67mV/°/s (Tolerance:±5%)
Housing assembly	Top and bottom platforms for housing actuators are 3D printed with PLA using MakerBot Replicator (Tolerance: XY positioning - 11 microns, Z positioning - 2.5 microns)
Spacers	For alignment of the isolation system, 3D printed (Tolerance: same as the housing assembly)
Springs	Stainless steel compression springs (Tolerance: information not available from vendor)
Current amplifier	In-house manufactured current amplifier operated in current mode (Tolerance: could not be ascertained)

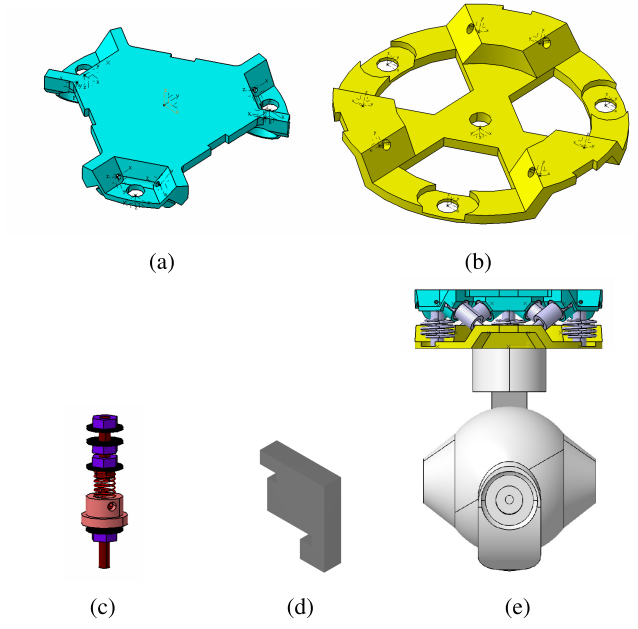

FIGURE 10. Prototype of the proposed active isolation system—(a) top platform, (b) bottom platform, (c) adjustable spring assembly, (d) spacer for alignment and (e) camera-isolation integrated system.

Let f be the forces in the legs of the isolation system. Based on principle of virtual work, the forces in the local frame of reference are related to the forces in the global frame of reference by the following equation

$$f^T \delta q = \begin{bmatrix} F & \tau \end{bmatrix}^T \delta x \implies \begin{bmatrix} F \\ \tau \end{bmatrix} = J^T f \tag{24}$$

F. DYNAMIC EQUILIBRIUM

The kinetic energy of the payload platform can be written as

$$T = \frac{1}{2} v^T m \mathbf{I} v + \frac{1}{2} \omega^T \mathbb{I} \omega \tag{25}$$

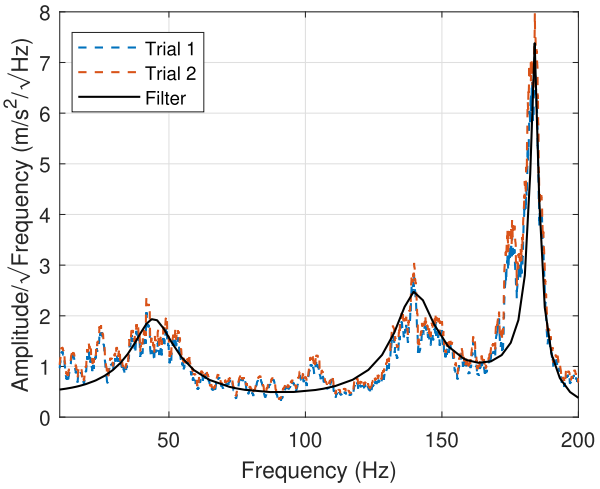

FIGURE 11. Drone spectrum in Z-direction.

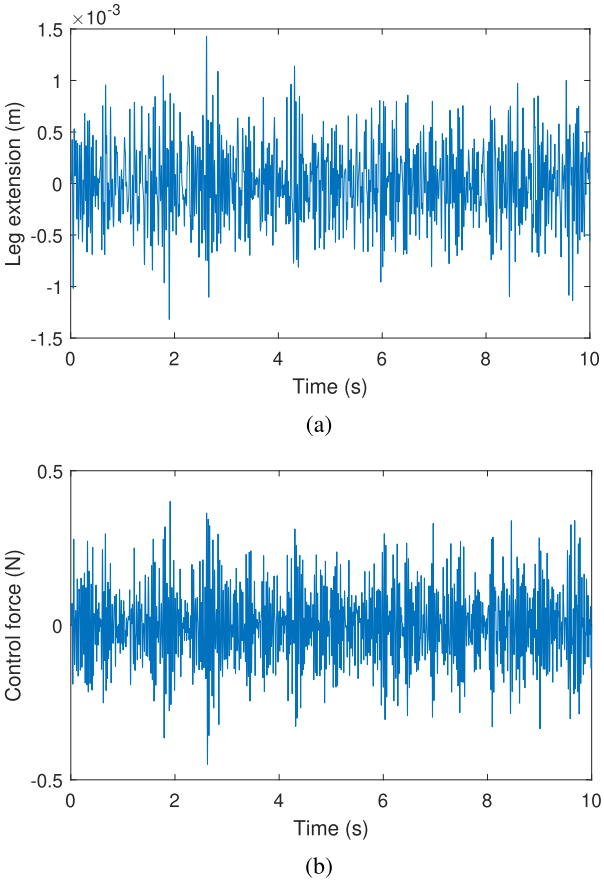

FIGURE 12. Response of isolation system when subjected to the external input corresponding to the drone spectrum-(a) leg extension and (b) control force.

where $\mathbb{I}$ is the moment of inertia and v is the absolute velocity of the payload platform in frame $\{B\}$. We neglect the stiffness of the platform and assume that the centre of mass of the payload coincides with the $\{P\}$ frame of reference. The translation velocity of the centre of mass of the payload plate

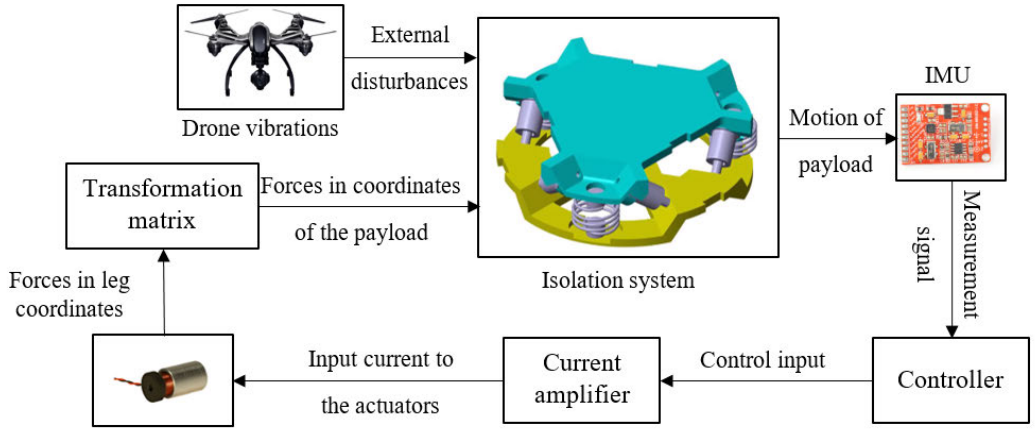

FIGURE 13. Control strategy for active stabilization.

can be written as

$$v = \left(\dot{x}, \dot{y}, \dot{z}\right)^T \tag{26}$$

The rotational part of the kinetic energy can be written as

$$\omega^T \mathbb{I} \omega = \mathbb{I}_x \dot{\theta}_x^2 + \mathbb{I}_y \dot{\theta}_y^2 + \mathbb{I}_z \dot{\theta}_z^2 \tag{27}$$

where $\mathbb{I}_x, \mathbb{I}_y, \mathbb{I}_z$ are the moment of inertia in frame $\{P\}$. The total kinetic energy of the payload (same as Equation 25) can be written in terms of global mass-inertia matrix, M, as

$$T = \frac{1}{2} \dot{X}^T M \dot{X} \tag{28}$$

The global mass matrix is obtained by equating the kinetic energies in Equations (25) and (28).

$$M = m.\text{diag}(1, 1, 1, R_x^2, R_y^2, R_z^2) \tag{29}$$

where m is the mass of the payload, R_x, R_y, R_z are the radii of gyration about the respective axis and diag(.) represent the diagonal matrix. Based on the spring assembly, the stiffness matrix of the platform is

$$K = \text{diag}(3k_h, 3k_h, 3k_v, 3k_v r^2/2, 3k_v r^2/2, 3k_h r^2) \tag{30}$$

The dynamic equilibrium equation of the isolator is given by

$$M\ddot{X} + KX = F_{ext} + J^T f \tag{31}$$

And if the base plate is subjected to the ground motion, the dynamic equation is

$$M\ddot{X} + KX = KX_b + J^T f \tag{32}$$

where X_b is the motion of the base plate in $\{P\}$ frame of reference.

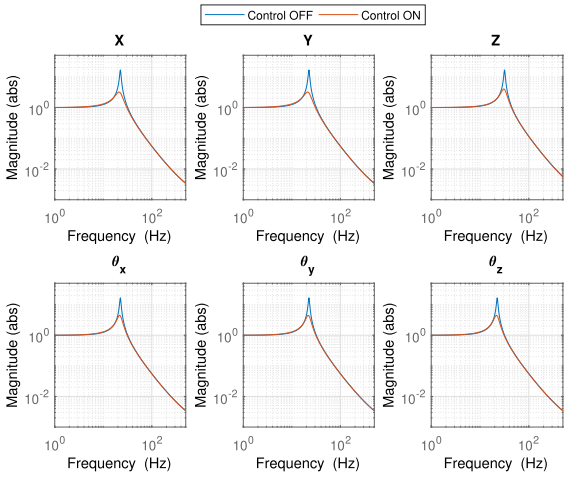

FIGURE 14. Transmissibility of the isolation system in different directions with and without active control.

IV. MECHANICAL PROTOTYPE

A prototype of the isolation system is designed and manufactured for experimental validation. This section gives an overview of the mechanical design. The different components of the isolation system are listed in Table 2. The prototype is designed to have a natural frequency at around 30 Hz in the vertical direction. The stiffness of the isolation in the horizontal direction is assumed to be half of that in the vertical direction. The damping ratio is assumed to be low (as there is no source of pure damping in the system) and taken as 1%. The different components and the assemblies are shown in Figure 10.

The first step in the design process is the choice of actuators. The isolation platform is intended for drone camera stabilization. Hence, it is important to characterize the vibrations coming from the drone. A typical drone spectrum in the Z-direction is shown in Figure 11 [32], [34]. The drone vibrations act as the external disturbances to the isolation system. Using centralized control (details follow in the next

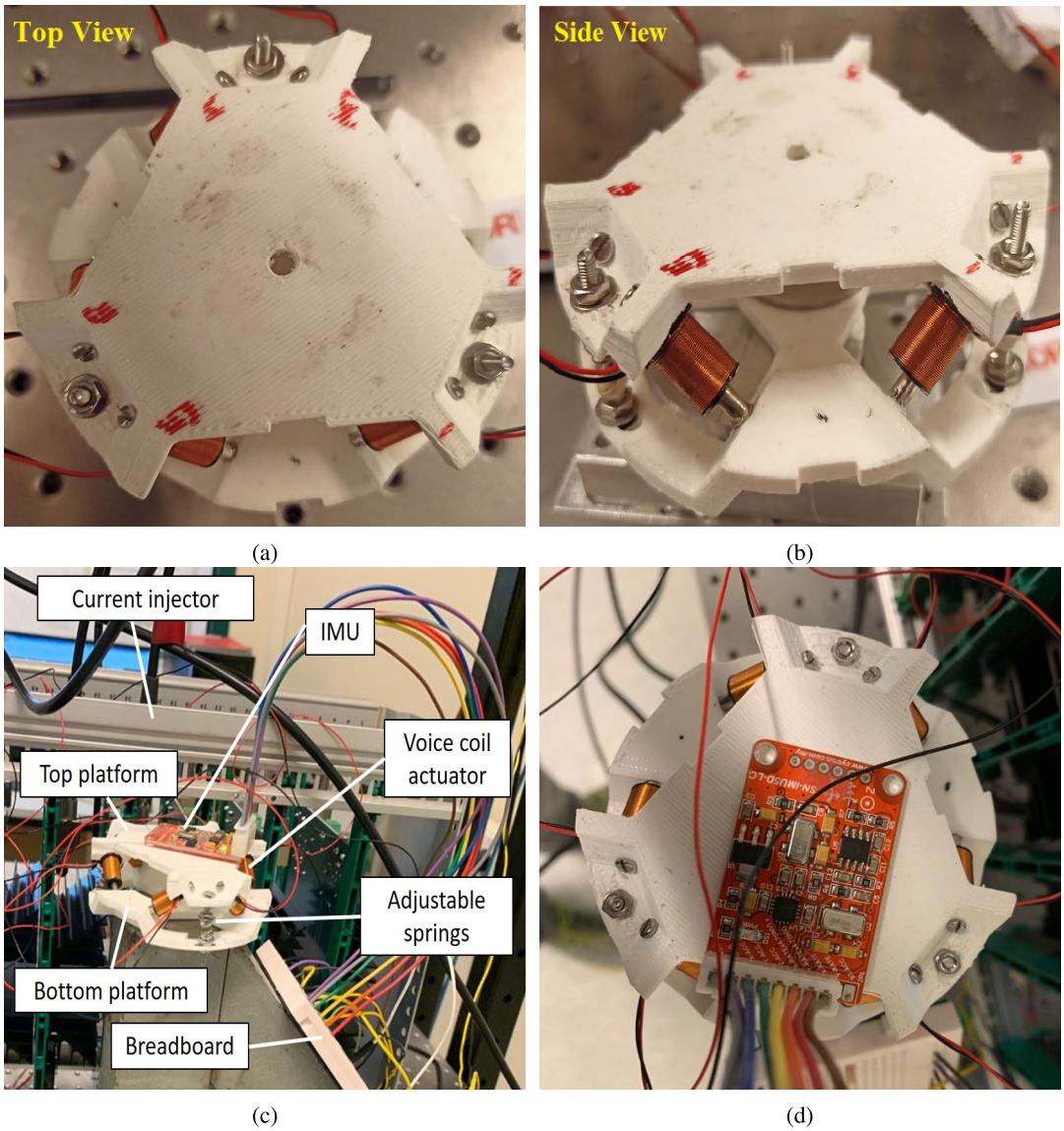

FIGURE 15. Experimental investigations—(a) top view of isolation system, (b) side view of isolation system, (c) experimental setup and (d) zoom-in view of the isolation system with IMU.

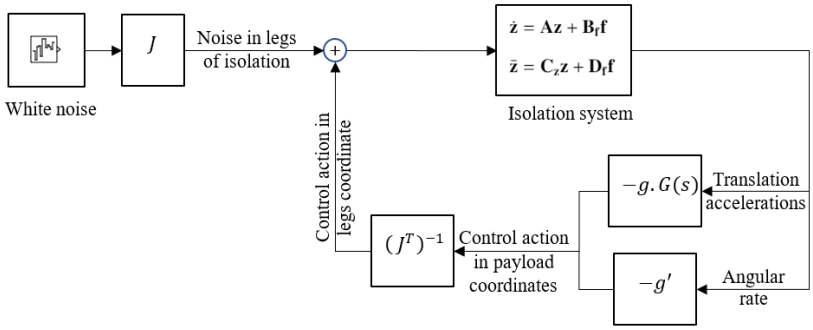

FIGURE 16. Block diagram for the experimental evaluation of the isolation performance.

section) with the dynamic model formulated in the previous section, the response is evaluated in terms of control force and leg extension. The response of the isolation system in shown in Figure 12. The actuators for the isolation system are selected based on force and stroke demand obtained from the preliminary analysis.

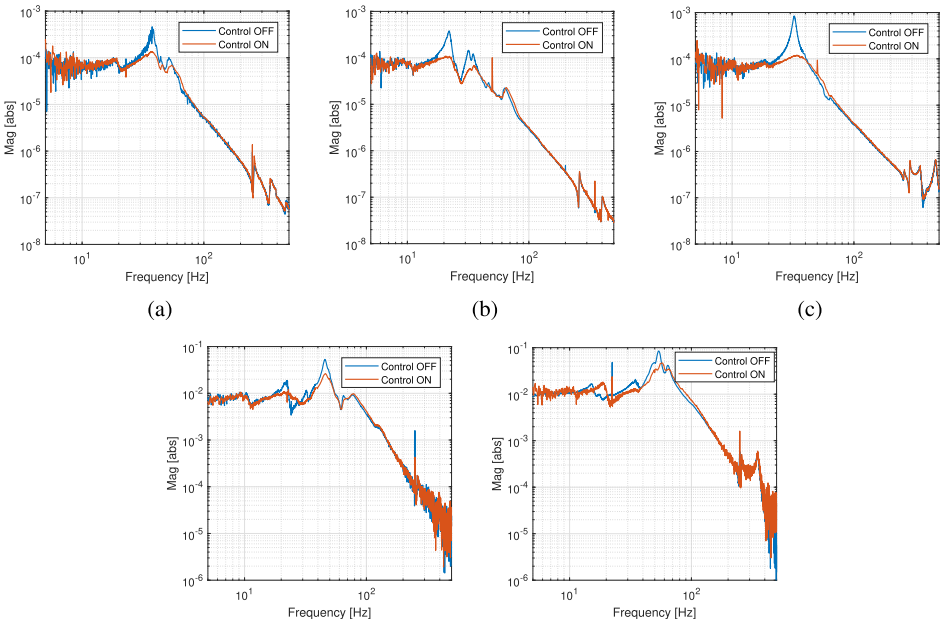

FIGURE 17. Response of the active isolation system with and without control in-(a) X-, (b) Y-, (c) Z-, (d) θ_X-and (e) θ_Y-directions.

It can also be seen from the drone spectrum that the vibrations are predominant between 150-200 Hz. Therefore, it is important to ensure that the flexible modes of the platforms are above 200 Hz. A finite element analysis of the top and bottom platform is carried out to identify the first couple of flexible modes. If the designed platform is found to have the flexible modes in the vicinity of frequency range of drone vibrations, the thickness of the platform should be increased to make it more stiff. Before manufacturing, it has been made sure that the flexible modes of the designed platform are above 200 Hz.

The top platform is supported on three springs which maintain the alignment of the non-contact voice coil actuators. This alignment can be disturbed when the payload is added on the top platform due to static deflection. Special fasteners are designed to compensate for this static deflection. The fasteners can be rotated to adjust the effective length and hence the stiffness of the spring. The nut is rotated until all the actuators are aligned in the mid-stroke position. The isolation system adds about 150g to the drone. The performance of the drone is not much affected due to the lightweight nature of the proposed isolation system.

Three spacers are designed to guide the spring adjustment. Once the spacers are fitted between the platforms, the cubic configuration is ensured and all the actuators are aligned perfectly. After this, the springs can be adjusted to ensure that the platforms remain in this configuration once the spacers are removed.

V. CONTROL DESIGN

In the present study, centralized control is used for active damping. The sensed output is the acceleration of the payload plate in three translation and three rotational directions. The block diagram for the control strategy is shown in Figure 13. The dynamics of the system in the state-space form which takes control force (f) and the external disturbance from the drone ($\ddot{w}$) as inputs, and inertial accelerations of the payload platform in six directions as output ($\bar{\mathbf{z}} = \ddot{X}$) can be written as

$$\begin{aligned} \dot{\mathbf{z}} &= \mathbf{A}\mathbf{z} + \mathbf{B_u}\mathbf{f} + \mathbf{B_w}\ddot{\mathbf{w}} \\ \bar{\mathbf{z}} &= \mathbf{C_z}\mathbf{z} + \mathbf{D_u}\mathbf{f} \end{aligned} \tag{33}$$

where

$$\mathbf{A} = \begin{bmatrix} \mathbf{0} & \mathbf{I} \\ -\mathbf{M^{-1}K} & -\mathbf{M^{-1}C} \end{bmatrix}, \quad B_u = \begin{bmatrix} \mathbf{0} \\ \mathbf{M^{-1}J^T} \end{bmatrix}, \; B_w = \begin{bmatrix} \mathbf{0} \\ -\mathbf{I} \end{bmatrix}$$
$$\mathbf{z} = \begin{bmatrix} \mathbf{X} \\ \dot{\mathbf{X}} \end{bmatrix}, \quad \mathbf{C_z} = \left[-\mathbf{M^{-1}K}, -\mathbf{M^{-1}C}\right], \; \mathbf{D_u} = \mathbf{M^{-1}J^T}.$$

In order to add damping to the system, the control force should be proportional to the velocity. Since payload platform acceleration is used as feedback, an integrator is used to obtain velocity from the feedback signal. However, this active damping does not degrade the high frequency response of the isolator and is effective in damping the resonance alone. The use of a pure integrator as a control can result in drift. In order to avoid the actuator saturation due to drift, a weak integrator is used instead. The controller for the isolation system is given by

$$G(s) = \frac{10\pi}{s + 10\pi} \tag{34}$$

The control input to the actuators is given by

$$\mathbf{f} = -G_m G(s) \cdot \ddot{\mathbf{X}} \tag{35}$$

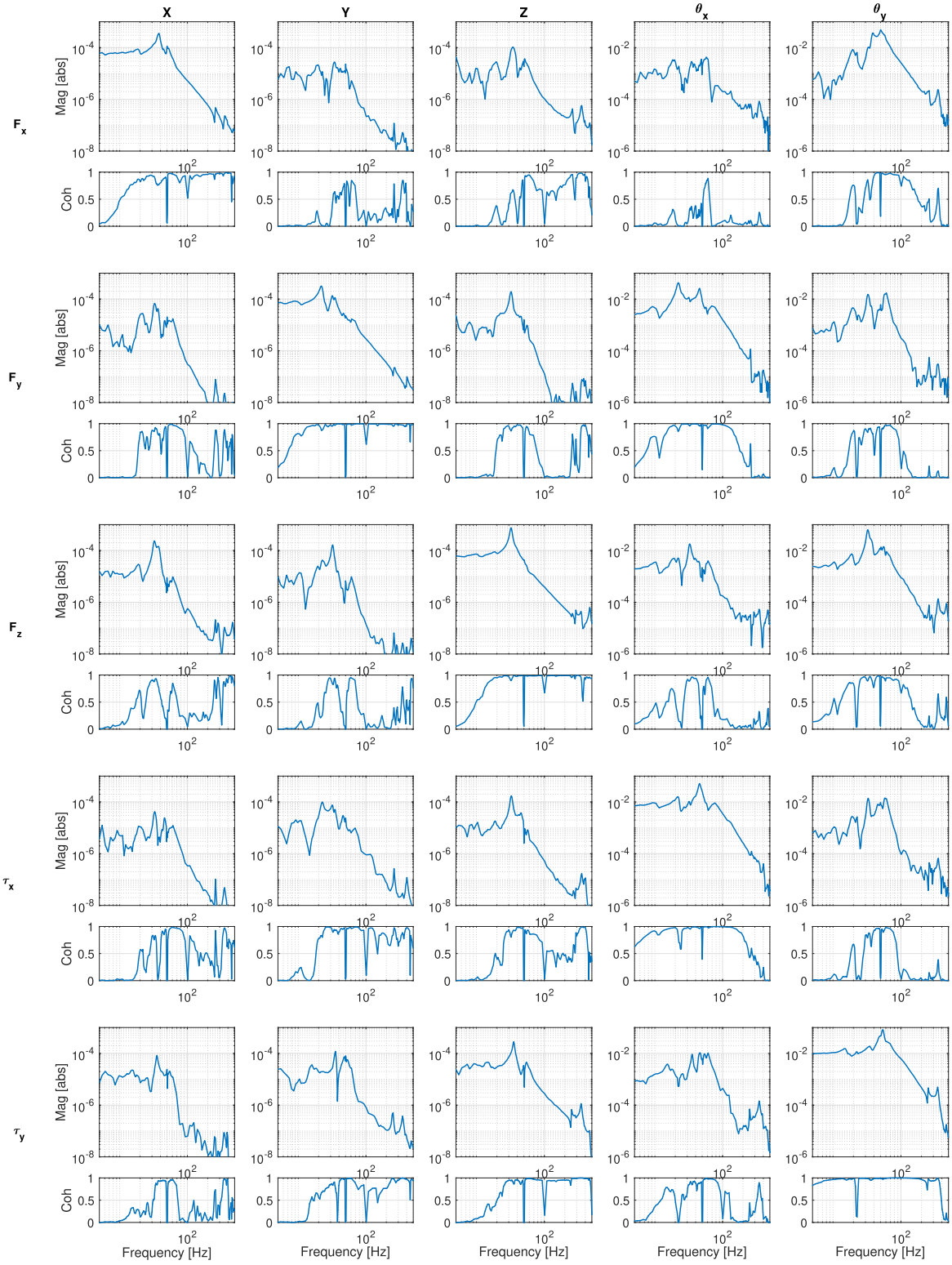

FIGURE 18. Cross coupling between different directions.

where $G_m = \text{diag}(g, g, g, g', g', g')$ is the controller gain matrix. The transmissibility of the isolation system with the controller gain matrix $G_m = \text{diag}(4, 4, 4, 0.004, 0.004, 0.004)$ is shown in Figure 14. It can be seen that the control strategy is able to reduce the isolator response near resonance without amplification at higher frequencies.

VI. EXPERIMENTAL INVESTIGATIONS

The controller designed in the previous section is validated experimentally. The details of the experimental setup and results are described below.

A. SETUP

The experimental setup used for the performance evaluation is shown in Figure 15. The bottom platform of the isolation system is bolted on a rigid support. In the experiments, the IMU unit is glued on the top platform of the prototype. For the actual system, the IMU can be encapsulated inside the isolator. The voice coil actuators are driven using the current amplifier. MicroLabBox from dSpace is used for the real-time implementation of the evaluated controller. A DC voltage source is used to power the IMU. The IMU used in the experiments measures five degrees of freedom — X-, Y-, Z-direction accelerations and angular rate about X- and Y-axis. Therefore, controller for the rotations about X- and Y-axis is replaced by a simple gain (instead of a weak integrator).

B. ISOLATION PERFORMANCE

The actuators of the isolation system are used for control as well as for injecting the external disturbances in the system (equivalent to forces and moments acting on the payload plate). The block diagram for the experiments is shown in Figure 16. The force and moment transmissibilities of the isolation system are shown in Figure 17. It can be seen that the control strategy is effective in response reduction of the system near resonance. This reduction in the response has not come at the expense of amplification at high frequency, unlike observed in the case of passive isolation. The isolation system was designed to have the resonance in Z-direction at around 30 Hz. The frequency of the isolator in Z-direction is found to be around 31 Hz. In the preliminary design, the horizontal stiffness of the isolation was assumed to be half of the vertical stiffness. Also, it was assumed that all the three springs have similar properties. However, this is not the case in the experiments. The frequency of the isolator in the X- and Y-directions is found to be around 38 Hz and 22 Hz, respectively. We can also observe more than one peak in the frequency response, suggesting the coupling between different directions. The frequency of the isolation in the θ_x- and θ_y-directions is found to be around 45 Hz and 50 Hz, respectively. Since, the lengths of the springs were adjusted in the lab, there was not enough precision. This difference in the mechanical properties of the springs is presumed to be the main reasons for the cross coupling between different directions. This cross coupling can be reduced by using springs manufactured with higher precision. The other probable reason for cross-coupling could be the parasitic stiffness due to the cables used for instrumentation or imperfect Jacobian due to misalignment. The isolation system also has a high frequency roll-off up to 200 Hz which makes it appropriate for drone camera stabilization. It should be noted that the active control is found to be effective even in the presence of the cross coupling.

C. CROSS COUPLING

The cross coupling between the different directions is measured by conducting five different experiments. In each of the experiments, the payload plate was subjected to force or moment in predominantly one direction. The response of the isolation system was recorded in all the directions. The results of the experiments are shown in Figure 18. Each row corresponds to one experiment in which the payload is subjected to either a force or a moment in a particular direction. Each column corresponds to the response of the isolation system in a particular direction. The magnitude plot alone is not sufficient to identify the cross coupling. Therefore, the coherence plot is also shown below the magnitude plot. The coherence plot shows the correlation between the applied force/moment and the response. It is observed that in the diagonal plots, the response is well correlated with the external input. Also, the magnitude is higher than the translations/rotations in the other directions. This indicates that the isolator was predominantly excited in one direction. From the coherence plots, it is observed that the there is cross coupling between $F_x - \theta_y$, $F_y - \theta_x$, $F_z - \theta_y$ and $\tau_y - Z$ directions. As described earlier, it is presumed to be due to the difference in stiffness of the three springs used in the isolation system.

VII. CONCLUDING REMARKS

A new multi-degree of freedom isolation system has been proposed for drone camera stabilization. The isolation system is based on a Stewart platform configuration. The legs of the isolation system are composed of non-contact voice coil actuators. This helps to avoid the spurious resonances in the legs. The isolation system is also devoid of flexible joints. This helps to avoid the problem of friction, backlash and parasitic stiffness. The top and the bottom platforms are connected using three springs. The control architecture uses an IMU with centralized control strategy. The parts of the isolation are manufactured using 3D printing technology. The isolation system has been designed considering the stroke and force demand for isolation from drone vibrations. The performance of the isolation system has been verified experimentally. The isolating system is found to be effective in response reduction of the payload platform without amplification at the higher frequencies. The cross coupling between different directions has also been observed in the experiments. This is attributed to the fact that the stiffness of the springs holding the top and bottom platforms are not identical. This cross coupling can be reduced by using industrial grade springs manufactured with higher precision. Nevertheless, the control strategy is found to perform well even in the presence of this cross coupling. Although the isolation system is proposed for drone camera stabilization, it can be extended to various other fields (like autonomous vehicles, precision agriculture or remote sensing) which require acquisition of high quality images.

REFERENCES

[1] A. M. Wahbeh, J. P. Caffrey, and S. F. Masri, "A vision-based approach for the direct measurement of displacements in vibrating systems," *Smart Mater. Struct.*, vol. 12, no. 5, p. 785, 2003.
[2] Y.-R. Chen, K. Chao, and M. S. Kim, "Machine vision technology for agricultural applications," *Comput. Electron. Agricult.*, vol. 36, nos. 2–3, pp. 173–191, 2002.
[3] M. A. Ma'sum, M. K. Arrofi, G. Jati, F. Arifin, M. N. Kurniawan, P. Mursanto, and W. Jatmiko, "Simulation of intelligent unmanned aerial vehicle (UAV) for military surveillance," in *Proc. Int. Conf. Adv. Comput. Sci. Inf. Syst. (ICACSIS)*, Sep. 2013, pp. 161–166.
[4] H. Xiang and L. Tian, "Development of a low-cost agricultural remote sensing system based on an autonomous unmanned aerial vehicle (UAV)," *Biosyst. Eng.*, vol. 108, no. 2, pp. 174–190, Feb. 2011.
[5] W. McFadden, "Vibration considerations for high performance camera systems," *Proc. SPIE*, vol. 0079, pp. 51–57, Sep. 1976.
[6] D. A. Kienholz, C. A. Smith, and W. B. Haile, "Magnetically damped vibration isolation system for a space shuttle payload," *Proc. SPIE*, vol. 2720, pp. 272–281, May 1996.
[7] K. Gjika and R. Dufour, "Rigid body and nonlinear mount identification: Application to onboard equipment with hysteretic suspension," *J. Vibrat. Control*, vol. 5, no. 1, pp. 75–94, Jan. 1999.
[8] R. Fernandez, A. Abolmaali, F. Kamangar, and T. Le, "Analysis and development of a passive mechanical vibration abatement device for traffic monitoring cameras," *J. Transp. Eng.*, vol. 135, no. 5, pp. 270–278, May 2009.
[9] Y. X. Qian, L. B. Yang, F. R. Hu, and X. T. Hong, "Design of stable image platform on airborne camera," *Adv. Mater. Res.*, vol. 314, pp. 2495–2498, Aug. 2011.
[10] A. E. Pete, D. Kress, M. A. Dimitrov, and D. Lentink, "The role of passive avian head stabilization in flapping flight," *J. Roy. Soc. Interface*, vol. 12, no. 110, Sep. 2015, Art. no. 20150508.
[11] A. L. Webster and W. H. Semke, "Broad-band viscoelastic rotational vibration control for remote sensing applications," *Model Anal.*, vol. 11, no. 11, pp. 1339–1356, 2005.
[12] J.-L. Maes, S. Binczak, and V. Lhenry, "A passive stabilization solution for camera embedded onboard small planes," in *Proc. Integr. Commun., Navigat. Surveill. Conf. (ICNS)*, Apr. 2014, p. U3-1.
[13] M. Verma, A. Pece, S. Hellegouarch, J. Watchi, G. Durand, S. Chesné, and C. Collette, "Dynamic stabilization of thin aperture light collector space telescope using active rods," *J. Astronomical Telescopes, Instrum., Syst.*, vol. 6, no. 1, 2020, Art. no. 014002.
[14] M. Verma, V. Lafarga, and C. Collette, "Perfect collocation using self-sensing electromagnetic actuator: Application to vibration control of flexible structures," *Sens. Actuators A, Phys.*, vol. 313, Oct. 2020, Art. no. 112210.
[15] M. Verma, T. Dehaeze, G. Zhao, J. Watchi, and C. Collette, "Virtual sensor fusion for high precision control," *Mech. Syst. Signal Process.*, vol. 150, Mar. 2021, Art. no. 107241.
[16] G. N. Marichal, M. Tomás-Rodríguez, Á. Hernández, S. Castillo-Rivera, and P. Campoy, "Vibration reduction for vision systems on board unmanned aerial vehicles using a neuro-fuzzy controller," *J. Vibrat. Control*, vol. 20, no. 15, pp. 2243–2253, Nov. 2014.
[17] K. J. Stuckel, W. H. Semke, N. Baer, and R. R. Schultz, "A high frequency stabilization system for UAS imaging payloads," in *Structural Dynamics*, vol. 3. New York, NY, USA: Springer, 2011, pp. 1411–1419.
[18] K. J. Stuckel and W. H. Semke, "A piezoelectric actuated stabilization mount for payloads onboard small UAS," in *Advanced Aerospace Applications*, vol. 1. New York, NY, USA: Springer, 2011, pp. 295–305.
[19] P. Sumathy, S. Indhumathi, V. Bhuvaneshwari, and A. Bhaskar, "Active vibration suppression of UAV camera mounts," *Indian J. Sci. Technol.*, vol. 9, no. 1, pp. 1–6, Jan. 2016.
[20] J.-S. Oh, Y.-M. Han, and S.-B. Choi, "Vibration control of a camera mount system for an unmanned aerial vehicle using piezostack actuators," *Smart Mater. Struct.*, vol. 20, no. 8, Aug. 2011, Art. no. 085020.
[21] J.-S. Oh, S.-B. Choi, H.-J. Cho, C.-H. Lee, and M.-W. Cho, "Performance evaluation on an active camera mount system for UAV via hardware-in-the-loop-simulation," *Trans. Korean Soc. Noise Vibrat. Eng.*, vol. 20, no. 8, pp. 767–773, 2010.
[22] D.-H. Park and S.-B. Choi, "Active vibration control of UAV EO/IR sensor mount using piezoelectric actuator," *Trans. Korean Soc. Noise Vibrat. Eng.*, vol. 18, no. 12, pp. 1278–1285, 2008.
[23] D.-O. Lee, L.-H. Kang, and J.-H. Han, "Active vibration isolation demonstration system using the piezoelectric unimorph with mechanically pre-stressed substrate," *J. Intell. Mater. Syst. Struct.*, vol. 22, no. 13, pp. 1399–1409, Sep. 2011.
[24] N. Baer and W. H. Semke, "A frictionless lightweight active vibration control mount for small UAS," in *Topics in Modal Analysis I*, vol. 5. New York, NY, USA: Springer, 2012, pp. 367–375.
[25] A. Gasteratos, "Active camera stabilization with a fuzzy-grey controller," *Eur. J. Mech. Environ. Eng*, vol. 2, pp. 18–20, 2009.
[26] A. Preumont, M. Horodinca, I. Romanescu, B. de Marneffe, M. Avraam, A. Deraemaeker, F. Bossens, and A. Abu Hanieh, "A six-axis single-stage active vibration isolator based on Stewart platform," *J. Sound Vibrat.*, vol. 300, nos. 3–5, pp. 644–661, Mar. 2007.
[27] Y. Zheng, Q. Li, B. Yan, Y. Luo, and X. Zhang, "A Stewart isolator with high-static-low-dynamic stiffness struts based on negative stiffness magnetic springs," *J. Sound Vib.*, vol. 422, pp. 390–408, May 2018.
[28] Z. Wu, X. Jing, B. Sun, and F. Li, "A 6DOF passive vibration isolator using X-shape supporting structures," *J. Sound Vib.*, vol. 380, pp. 90–111, Oct. 2016.
[29] Q. He, C. Zeng, Z. Gao, and Z. Wu, "Analysis and design of the Stewart platform-based parallel support bumper for inertially stabilized platforms," *IEEE Trans. Ind. Electron.*, vol. 67, no. 5, pp. 4203–4215, May 2020.
[30] C. Wang, X. Xie, Y. Chen, and Z. Zhang, "Investigation on active vibration isolation of a Stewart platform with piezoelectric actuators," *J. Sound Vib.*, vol. 383, pp. 1–19, Nov. 2016.
[31] X. Yang, H. Wu, B. Chen, S. Kang, and S. Cheng, "Dynamic modeling and decoupled control of a flexible Stewart platform for vibration isolation," *J. Sound Vib.*, vol. 439, pp. 398–412, Jan. 2019.
[32] M. Verma, V. Lafarga, M. Baron, and C. Collette, "Active stabilization of unmanned aerial vehicle imaging platform," *J. Vib. Control*, vol. 26, nos. 19–20, pp. 1791–1803, 2020.
[33] A. A. Hanieh, "Active isolation and damping of vibrations via Stewart platform," Ph.D. dissertation, Act. Struct. Lab., Université Libre de Bruxelles, Brussels, Belgium, 2003.
[34] M. Verma and C. Collette, "Active vibration isolation system for drone cameras," in *Proc. Int. Conf. Vib. Problems*, Crete, Greece, 2019, p. 18795.

MOHIT VERMA received the Ph.D. degree in structural engineering from the AcSIR, India. After that, he joined the Precision Mechatronics Laboratory, Université Libre de Bruxelles (ULB), Belgium, as a Postdoctoral Research Associate. He has been working as a Scientist at the CSIR-Structural Engineering Research Centre since 2011. His research interest includes the vibration control of structures.

VICENTE LAFARGA is currently pursuing the Ph.D. degree with the Precision Mechatronics Laboratory, Université Libre de Bruxelles (ULB). He is also working toward the development of a hybrid isolation system for space applications. His doctoral study was funded by the European Space Agency (ESA) through an NPI Program. His research interests include payload isolation from the launcher environment.

THOMAS DEHAEZE is currently pursuing the Ph.D. degree with the University of Liège. He has also been working at the ESRF, France, since 2017. His doctoral study was funded by the FRIA grant. His research interests include the development of mechatronics concepts and their applications for a nano-positioning end station.

CHRISTOPHE COLLETTE received the M.Sc. and Ph.D. degrees in mechanical engineering from the Université Libre de Bruxelles (ULB), in 2003 and 2007, respectively. He is a Professor of Mechatronics with the Faculty of Engineering, ULB, and the University of Liège. He is the Director of the Precision Mechatronics Laboratory. His main research interests include the active and passive control of vibration, optical inertial sensors, and future space telescopes.